IMPROVED CLIMATOLOGIES OF LOWER AND MIDDLE ATMOSPHERIC GRAVITY WAVE ACTIVITY AT MARS.

N.G. Heavens, *Space Science Institute, Boulder, CO, USA and London, UK (nheavens@spacescience.org)*, **A. Pankine,** *Space Science Institute*, **J.M. Battalio,** *Earth and Planetary Sciences, Yale University*, **C.J. Wright,** *Centre for Space, Atmospheric and Oceanic Science, University of Bath*, **D.M. Kass, A. Kleinboehl, S. Piqueux,** *NASA Jet Propulsion Laboratory, Caltech*, **J.T. Schofield,** *JPL, Retired*.

Introduction

Atmospheric gravity waves (GW) are excited by impulses in the atmospheric circulation; like the movement of the wind over and around topography, jet stream meanderings, and convective activity. [1, 2, 3]. GW transfer energy and momentum through stable atmospheric regions and thereby couple different levels of the atmosphere or different mesoscale weather systems [e.g., 4, 5, 6, 1, 7, 3]. In Mars's atmosphere, GW seem to modulate the intensity of middle atmospheric downwelling near the poles, the escape of constituents from the upper atmosphere, and even the formation of mesoscale cloud trails in the middle atmosphere [8, 9, 10].

GW processes are increasingly parameterized within Mars general circulation/global climate models (GCM) [e.g., 11, 12, 13, 14, 8]. These parameterizations largely derive from ones originally applied to and/or validated at the Earth and often have been validated by or tuned to reproduce the zonal mean temperature structure of the middle atmosphere [e.g., 11, 8], which can be significantly affected by mechanisms other than GW [15, 16, 17]. Another approach to parameterization development and evaluation has been to resolve GW explicitly in higher resolution simulations [18, 19, 20, 21]. Observational validation of parameterized and resolved GW forcing, however, has been limited.

The first purpose of this abstract is to provide a short, integrated overview of the growing body of satellite observations of GW activity in Mars's lower and middle atmosphere that can aid direct understanding of GW dynamics and validate modeling. Along the way, we will highlight important results from a project currently funded by NASA to expand climatologies of GW activity. These results would be the focus of our conference presentation. Where appropriate, this discussion also will consider complementary information from observations of upper atmospheric GW activity [e.g., 22, 23, 24, 25, 26, 27, 10, 28]. Note also the increasing study of GW in surface weather observations [e.g., 29, 30].

History and types of observations

GW are fundamentally waves whose restoring force is buoyancy. As they propagate, they perturb the temperature, wind, pressure, and density fields locally [1]. Their periods range from the inverse of the Brunt-Väisälä frequency to the inverse of the Coriolis frequency. Martian atmospheric scientists generally are familiar with some aspects of GW theory, because thermal tides can be read and mathematically treated as both planetary waves and GW [e.g., 31]. And so GW were first recognized as not quite tidal oscillations within the entry profiles of the Viking landers [32]. GW also were recognized as the cause of lee wave clouds [33, 34].

Quantitative study of GW in the lower and middle atmosphere has largely focused on extracting GW signals from observations of temperature variability. Many studies have been based on studies of individual profiles, generally using occultations to produce temperature profiles that are loosely analogous to entry profiles, just far more frequently and inexpensively collected. GW activity in the lower atmosphere has been sensed using radio occultation [35, 36]. A broader vertical range has been accessed by ground-based stellar occultation [37], stellar occultation in Mars orbit [38], and solar occultation in Mars orbit [39]. Recent studies by [38] and [39] rely on temperature profiles that approximate the broad lower to upper atmosphere range (from 20 to 120/160 km), vertical resolution, and temperature uncertainty of entry profiles. The main downside is that occultations are usually limited to < 10 per day, making it difficult to isolate GW sources in map view. Single profile studies also can sense convective instabilities associated with GW growing to an unstable amplitude, breaking, and depositing its momentum [35, 40, 41, 38, 39].

Other studies have looked at horizontal variability in temperature/brightness temperature, usually along the dimension of spacecraft travel. In rare cases, GW have been imaged, either in near-infrared dayglow by OMEGA on board Mars Express [42] or in Mars Odyssey THEMIS Band 10 imagery, which looks near the center of the 15 μm CO_2 band [43] (Fig. 1. The 15 μm CO_2 band is also regularly measured by mapping spectrometers/radiometers like MGS-TES and MRO-MCS, and GW signals have been inferred or explicitly searched for in data from these instruments [44, 45, 46, 47, 48]. As we will see in the next section, looking at multiple angles and at different baselines allows different portions of the GW spectrum to be observed. Another advantage of studying horizontal variability is the high data density possible, typically more than two orders of magnitude greater than possible due to occultation [47].

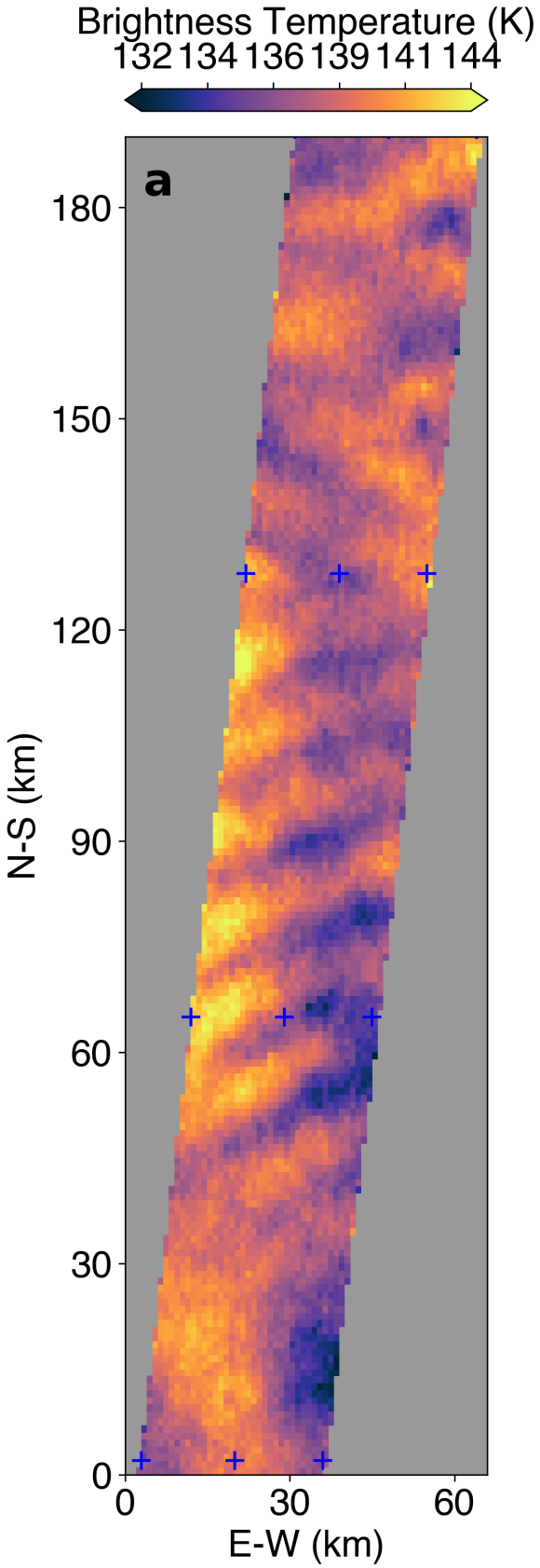

Figure 1: Example of GW activity in ODY-THEMIS Band 10 imagery reprocessed as described in [43](Battalio et al., this meeting). The 25 km horizontal wavelength waves propagating along the northwest to southeast direction between 40 and 130 km on the north-south axis are most obvious, but a mixture of other wavelength modes is also present.

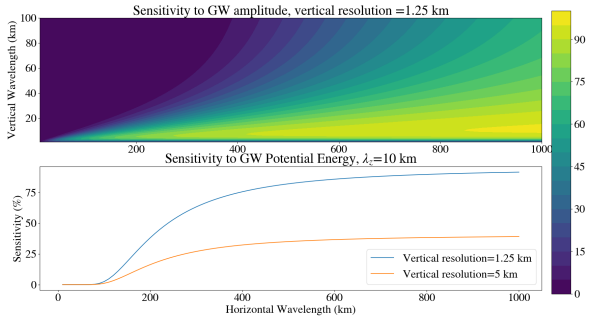

Figure 2: Theoretical sensitivity of limb observations to GW activity following [49]. (a) Sensitivity to amplitude (%) for an observation with a vertical resolution of 1.25 km, as in [35]. Note that [35] filtered out vertical wavelengths > 10 km; (b) Sensitivity to GW potential energy (%) for observations at two vertical resolutions at a vertical wavelength of 10 km.

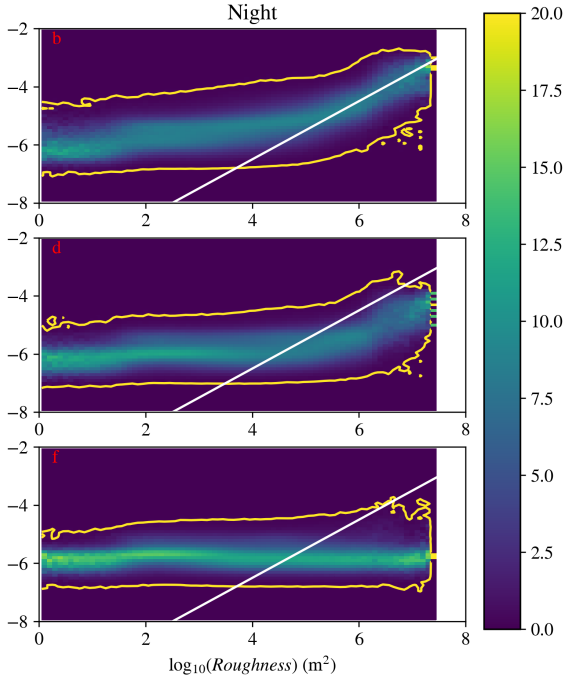

Figure 3: Probability distributions of GW activity as a function of surface roughness in MCS channels sensitive to GW in broad vertical ranges centered at 5 km (A1, top panel), 15 km (A2, middle panel), 25 km (A3, bottom panel). The white line is a fit line appropriate for orographic GW activity associated with wind speeds of 1.5 to 3 ms^{-1}, or perhaps larger, depending on the exact form of interaction with topography. Originally published in [48].

The observational filter

Any type of GW observation only sees a portion of the GW spectrum at one time. It is only by combining these different sources of information that a more complete picture emerges [e.g., 50, 51]. This concept is known as the observational filter.

For occultation-based single profile observations (approximated as limb observations), the filter is biased toward long horizontal wavelengths and short vertical wavelengths [52, 49] (Fig. 2a). By applying Eq. 1 of [49], it is possible to show that GW with horizontal wavelengths < 100 km are largely invisible to occultation profiles (Fig. 2b). Single profile observations are not necessarily dominated by GW with horizontal wavelengths < 400 km; such GW just contribute more to the signal. However, the invisibility of short horizontal wavelength waves may be consequential for evaluating GW dynamical effects; GW momentum flux is inversely proportional to horizontal wavelength [53]. Single profile studies also generally must select some portion of the vertical wavelength spectrum (usually < 10 or 15 km in order to extract GW distinct from tidal signals) [35, 39]. So a short period GW population with long vertical wavelengths will be invisible. Note that momentum flux is proportional to vertical wavelength [53].

The main controls on multiple profile studies are angle and baseline. Nadir observations are sensitive to long vertical wavelengths, while more glancing angles can access shorter vertical wavelengths [48]. In the case of MRO-MCS (and to a lesser extent for MGS-TES), radiance observations are discontinuous. Such observations create baselines along which temperature variability can be measured. These baselines effectively remove the sensitivity of the observations to longer horizontal wavelengths. Shorter horizontal wavelengths can be excluded by averaging. Judicious attention to these considerations can allow particular parts of the spectrum to be narrowly targeted. So for example, 27 continuous limb scans using MRO-MCS can produce weak sensitivity (no more than 30% in amplitude) to GW activity narrowly targeted at 100 to 200 km horizontal wavelength and near 5 km vertical wavelength. However, caution must be exercised when relying on such weak sensitivity, because a reduced signal may be overpowered by instrumental noise.

The orographic source dominates near the surface

One important source of GW is the interaction of wind with topography, commonly known as the orographic source. Crucially, such waves tend to have phase velocities close to zero, making it difficult for them to propagate through an environment with light winds, Mars's significant relief suggested orographic GW would be common on Mars, a hypothesis first explored but not confirmed by [35].

Using MRO-MCS off-nadir observations to look in the first scale height, we were able to demonstrate that GW activity close to the surface is a strong function of roughness in high roughness areas [48]. The slope of this relationship is theoretically predictable and consistent with a reasonable range of surface wind speeds (Fig. 3.). This relationship breaks down by an altitude of ≈ 25 km, suggesting orographic waves are strongly filtered in the lower atmosphere, partly explaining why this relationship was hard to see in the 10 to 30 km altitude band sampled by [35]. But data density also was important. $\approx 6.5 \times 10^6$ measurements were used to make Fig. 3, while [35] was based on 7917 profiles.

Seasonal shifts in GW activity

One very simple result that has fallen out of multiple datasets are seasonal shifts of GW activity between hemispheres. These datasets do not always agree, though. [35] found that southern tropical GW activity weakened during its summer, whereas [47, 38] found the opposite. [47] also found that high GW activity in the extratropics shifted between hemispheres during their respective winters.

Dust storms radically change GW activity

One surprising result from surveying off-nadir observations from MRO-MCS was that GW activity decreased during dust storm activity, particularly during the planet-encircling dust event of MY 34 (hereafter 34P) [47]. This effect was particularly apparent in areas of lower GW activity in the tropics. These areas tend to be smoother and so are likely sources of non-orographic waves from dry convection. Areas of high GW activity in the extratropics were minimally affected. GW activity also seems to increase locally in the tropics [47, 48].

GCM simulations of explicitly resolved GW also predicted such a decrease, which is caused by suppression of convection and baroclinic activity by reduced surface heating due to high dust opacity [21]. Comparison with [47] suggested that modeling was underestimating the decrease, but re-examination of this work has accounted for the effects of opacity raising the vertical sensitivity range of the MCS channels [48]. Taking this effect into account, the factor of 2 decrease predicted by modeling now agrees with the observations, though some discrepancies in the spatial distribution of the effect still may remain and possibly may be explained by differences in the part of the GW spectrum being sampled by the observations and the modeling [21].

One other prediction of [21] is that dust storm activity would improve GW propagation to the middle atmosphere and result in increased middle atmospheric GW activity there. This result could explain enhancement of upper atmospheric GW activity during 34P [10, 9]. And indeed [48] showed that GW propagation in the trop-

ics did improve significantly during 34P. Decreased GW activity in the lower atmosphere resulted from reduced source strength near the surface. A preliminary analysis of lower and middle atmospheric GW activity from MRO-MCS limb observations only found reduced lower atmospheric GW activity during the planet-encircling dust event in MY 28 (28P), but we expect to present an improved analysis at this meeting.

A mesoscale peak in GW activity

As noted above, GW with shorter horizontal wavelengths and longer vertical wavelengths should dominate momentum transport. MGS-TES nadir observations have enabled us to characterize the horizontal wavelength spectrum of long vertical wavelength GW. As also found by a similar analysis by [44], we find that GW energy seems to peak at horizontal wavelengths $<$ 100 km. These short horizontal wavelengths also seem to be less filtered as they propagate in the lower atmosphere. There is also a clear scale separation between variability at $<$ 300 km horizontal wavelength and $>$ 1000 km horizontal wavelength population that can be attributed to tides and planetary waves.

There are two main implications of this result. First, observational techniques that focus on the shorter horizontal wavelength end of the spectrum provide a more accurate view of the dynamically significant GW population. Second, the lower atmospheric wave population peaks at somewhat shorter horizontal wavelength than the upper atmospheric population ($<$ 100 km vs. 100 to 300 or 500 km) as inferred by [22, 24, 54], either suggesting strong filtering of the short end of the population or that upper atmospheric GW are a secondary population produced by GW breaking below the upper atmosphere.

Acknowledgments

This work was funded by NASA's Mars Data Analysis Program (80NSSC19K1215). Work at the Jet Propulsion Laboratory, California Institute of Technology, was performed under a contract with the National Aeronautics and Space Administration. US Government sponsorship is acknowledged.

References: **[1]** D. C. Fritts and M. J. Alexander. In: *Rev. Geophys.* 41.1 (2003), pp. 3571–3589. **[2]** S. C. R. Rafkin. In: *JGR* 114 (2009), E01009. **[3]** A. S. Medvedev and E. Yiğit. In: *Atmosphere* 10.9 (2019). **[4]** S. E. Koch and P. B. Dorian. In: *Monthly Weather Review* 116.12 (1988), pp. 2570–2592. **[5]** J. R. Holton et al. In: *Rev. Geophys.* 33.4 (1995), pp. 403–439. **[6]** M. Yamanaka. In: *Adv. Space. Res.* 15.4 (1995), pp. 47–50. **[7]** E. Yiğit and A. S. Medvedev. In: *Adv. Space Res.* 55.4 (2015), pp. 983–1003. **[8]** G. Gilli et al. In: *JGR Planets* 125.3 (2020), e2018JE005873. **[9]** E. Yiğit et al. In: *GRL* 48.5 (2021), e2020GL092095. **[10]** V. Leelavathi, N. Venkateswara Rao, and S. V. B. Rao. In: *JGR Planets* 125.12 (2020), e2020JE006649. **[11]** F. Forget et al. In: *JGR* 104.E10 (1999), pp. 24155–24176. **[12]** A. Akingunola. PhD thesis. York University, Canada, 2009. **[13]** T. Kuroda et al. In: *J. Meteor. Soc. Japan Ser. II* 87.5 (2009), pp. 913–921. **[14]** A. S. Medvedev and E. Yiğit. In: *GRL* 39, L05201 (2012), p. L05201. **[15]** R. J. Wilson et al. In: *GRL* 35, L07202 (2008), p. L07202. **[16]** N. G. Heavens et al. In: *JGR Planets* 116.E1 (2011). **[17]** T. McDunn et al. In: *JGR Planets* 118.2 (2013), pp. 161–178. **[18]** T. Kuroda et al. In: *GRL* 42 (2015), pp. 9213–9222. **[19]** T. Kuroda et al. In: *JAS* 73.12 (2016), pp. 4895–4909. **[20]** T. Kuroda, E. Yiğit, and A. S. Medvedev. In: *JGR Planets* 124.6 (2019), pp. 1618–1632. **[21]** T. Kuroda, A. S. Medvedev, and E. Yiğit. In: *JGR Planets* 125.11 (2020), e2020JE006556. **[22]** J. E. Creasey, J. M. Forbes, and G. M. Keating. In: *GRL* 33, L22814 (2006), p. L22814. **[23]** S. L. England et al. In: *JGR Space Physics* 122.2 (2017), pp. 2310–2335. **[24]** A. Siddle et al. In: *Icarus* 333 (2019), pp. 12–21. **[25]** H. N. Williamson et al. In: *Icarus* 331 (2019), pp. 110–115. **[26]** J. Liu, S. Jin, and Y. Li. In: *JGR Space Physics* 124.11 (2019), pp. 9315–9334. **[27]** M. K. Elrod et al. In: *Ninth International Conference on Mars, Pasadena, California, USA, 22-25 July 2019*. 2019. **[28]** E. Yiğit et al. In: *GRL* n/a.n/a (2020), e2020GL092095. **[29]** D. Banfield et al. In: *Nature Geoscience* 13.3 (2020), pp. 190–198. **[30]** S. D. Guzewich et al. In: *JGR Planets* 126.8 (2021). **[31]** Z. Wu et al. In: *Nature Communications* 11.1 (2020). **[32]** A. Seiff. In: *Adv. Space Res.* 2.2 (1982), pp. 3–17. **[33]** R. Kahn. In: *JGR* 89.A8 (1984), pp. 6671–6688. **[34]** G. H. Pettengill and P. G. Ford. In: *GRL* 27.5 (2000), pp. 609–612. **[35]** J. E. Creasey, J. M. Forbes, and D. P. Hinson. In: *GRL* 33, L01803 (2006), p. L01803. **[36]** S. Tellmann et al. In: *JGR* 118 (2013), pp. 306–320. **[37]** W. R. Saunders, M. J. Person, and P. Withers. In: *The Astronomical Journal* 161.6 (2021), p. 280. **[38]** H. Nakagawa et al. In: *JGR Planets* 125.9 (2020), e2020JE006481. **[39]** E. D. Starichenko et al. In: *JGR Planets* 126.8 (2021), e2021JE006899. **[40]** N. G. Heavens et al. In: *GRL* 37.18 (2010). **[41]** M. Vals et al. In: *PSS* 178 (2019), p. 104708. **[42]** F. Altieri et al. In: *JGR* 117, E00J08 (2012), E00J08. **[43]** J. Battalio et al. In: *Bulletin of the AAS* 52.6 (Oct. 26, 2020). **[44]** T. Imamura, Y. Kawasaki, and T. Fukuhara. In: *JAS* 64.5 (2007), pp. 1717–1726. **[45]** C. J. Wright. In: *Icarus* 219 (2012), pp. 274–282. **[46]** A. G. Feofilov et al. In: *Icarus* 221.2 (2012), pp. 949–959. **[47]** N. G. Heavens et al. In: *Icarus* 341 (2020), p. 113630. **[48]** N. G. Heavens et al. In: *PSJ* 3.3 (2022), p. 57. **[49]** Q. T. Trinh et al. In: *Atmospheric Measurement Techniques* 8.3 (2015), pp. 1491–1517. **[50]** D. L. Wu and S. D. Eckermann. In: *JAS* 65.12 (2008), pp. 3695–3718. **[51]** M. J. Alexander et al. In: *Journal of Geophysical Research: Atmospheres* 113.D15 (2008). **[52]** P. Preusse et al. In: *Journal of Geophysical Research: Atmospheres* 107.D23 (2002), CRI 6-1-CRI 6–23. **[53]** M. Ern et al. In: *JGR* 109, D20103 (2004), p. D20103. **[54]** N. Terada et al. In: *JGR Space Physics* 122.2 (2017), pp. 2374–2397.